Applied Catalysis B: Environmental 123–124 (2012) 127–133

Contents lists available at SciVerse ScienceDirect

Applied Catalysis B: Environmental

journal homepage: www.elsevier.com/locate/apcatb

Formation of core/shell structured polystyrene/anatase TiO_2 photocatalyst via vapor phase hydrolysis

Fuzhi Shi[a], Yaogang Li[b], Hongzhi Wang[a,*], Qinghong Zhang[b,*]

[a] State Key Laboratory for Modification of Chemical Fibers and Polymer Materials, Donghua University, Shanghai 201620, PR China
[b] Engineering Research Center of Advanced Glasses Manufacturing Technology, MOE, Donghua University, Shanghai 201620, PR China

ARTICLE INFO

Article history:
Received 8 February 2012
Received in revised form 17 April 2012
Accepted 22 April 2012
Available online 26 April 2012

Keywords:
Polystyrene/TiO_2
Vapor phase hydrolysis
Photocatalysis
Phenol
Stability

ABSTRACT

The core/shell structured polystyrene/anatase TiO_2 (PS/A-TiO_2) photocatalyst is prepared via vapor phase hydrolysis method and characterized by X-ray diffraction, transmission electron microscopy (TEM), High resolution transmission electron microscopy (HRTEM), thermogravimetry, N_2 adsorption/desorption isotherm analysis and UV–vis spectra. TEM and HRTEM show that well crystalline A-TiO_2 nanocrystals are immobilized on the surface of PS microspheres with dimensions of 400 nm. The TiO_2 crystallite size in the shell ranges from 7.5 nm to 13.6 nm, which is dependent on the temperature of vapor phase hydrolysis. The weight ratio of A-TiO_2 in the composite can be tuned by varying the content of titanium precursor. The composite density is lower than that of bare A-TiO_2 because of the light PS core, thus the composite has improved floating property. The photocatalytic performances of various catalysts in the degradation of methylene blue (MB) and phenol are evaluated, and the core/shell catalyst has a relatively higher activity than that of bare A-TiO_2 due to the improved floating and light harvesting ability. However, the PS core competitively consumes some active radicals, which are generally essential to the photocatalytic oxidation of MB, phenol or their intermediate derivatives. Then an insulating coating of SiO_2 between the PS core and A-TiO_2 shell is also introduced via vapor phase hydrolysis process, and the long-term stability of core/shell structured composite is enhanced.

1. Introduction

In recent years, the strategy to fabricate nanocoating or shell on colloidal particles is of burgeoning interest [1–6], because such particles combine the advantages of organic materials such as low density, transparency, low refractive index with the special functions of inorganic solids. Titania-related core/shell particles have been extensively investigated due to their promising application in filler, drug delivery system, photocatalysis and solar energy conversion [7–14]. Most of the core/shell structured polymer/titania microspheres are prepared via layer-by-layer (LbL) assembly, micro-emulsion polymerization, chemical vapor deposition and sol–gel technique [15–18]. However, most titania shells fabricated by these methods are amorphous nature [19–21], which limits their use in photocatalysis, solar energy conversion and other applications. Calcination above 500 °C is usually needed to crystallize these amorphous solids and hollow titania spheres with poor mechanical strength are obtained. LbL assembly is an alternative way to fabricate polycrystalline TiO_2 shell on the surface of polymer microspheres, but the polyelectrolyte employed in LbL process may be detrimental to both photocatalytic and antibacterial properties.

The aqueous sol–gel chemistry is rather complex, predominantly due to the high reactivity of the metal oxide precursor and the double role of water as both ligand and solvent [22]. In many cases, hydrolysis, condensation and aggregation occur almost simultaneously, hence, a slight variation in experimental condition could result in significantly morphology changes and serious issues regarding the reproducibility. Domen et al. [23] reported an ordered mesoporous niobium and tantalum mixed oxide was obtained via aging $NbCl_5$ and $TaCl_5$ alcohol solution in a controlled humidity atmosphere. Niederberger [24] developed a nonaqueous sol–gel route to prepare the discrete nanoparticles with phase and shape control. It has attracted much attention throughout chemical and material research fields by the controlled hydrolysis of titanium alkoxide and the shape-tuned synthesis of TiO_2 nanocrystals with unique property [25–29].

In this work, we report a strategy to prepare PS/A-TiO_2 core/shell structured microspheres via vapor phase hydrolysis (VPH) of titanium alkoxide. It is crucial that TiO_2 in the shell is perfectly crystallized without calcination in view of the poor thermal stability of PS. The VPH method combines the water molecules gently contacting with alkoxide in vapor form with the advantage of hydrothermal treatment to obtain highly crystallized TiO_2.

* Corresponding authors. Tel.: +86 21 67792943; fax: +86 21 67792855.
E-mail addresses: wanghz@dhu.edu.cn (H. Wang), zhangqh@dhu.edu.cn (Q. Zhang).

0926-3373/$ – see front matter © 2012 Elsevier B.V. All rights reserved.
http://dx.doi.org/10.1016/j.apcatb.2012.04.032

Table 1
Typical experiment recipes.

Sample	PS (g)	TBOT (μL)	Temperature (°C)
A	0.07	160	110
B	0.07	160	120
C	0.07	160	150
D	0.07	100	150
E	0.07	240	150

The size and crystallinity of A-TiO_2 crystallite in the composite could be tuned by varying the reaction temperature. The PS core possesses low density, transparency, flexibility, and awards PS/A-TiO_2 improved floatation, light harvesting property and higher photocatalytic activity than bare A-TiO_2. However, the recycle experiment in phenol indicates the PS core consumes some active radicals. Then an insulating coating of SiO_2 between the PS core and A-TiO_2 shell is also introduced via VPH. The final degradation ratio of phenol photocatalyzed by PS/SiO_2/A-TiO_2 has no changes during the 5 cycles. This also demonstrates the PS in PS/A-TiO_2 composite has competitively consumed some active radicals, which resulted in the less radicals be available to the photocatalytic oxidation of MB, phenol or their intermediate derivatives.

2. Experimental

2.1. Materials

Tetrabutyl titanate (TBOT), styrene (St), tetraethyl orthosilicate (TEOS), absolute ethanol and polyvinylpyrrolidone (PVP) K30 (Mw ≈4400–5400) were purchased from Shanghai Chemical Regent Co., China. Cationic initiator 2,2-azobis-(isobutyramidine) dihydrochloride (AIBA) was obtained from Aldrich. All chemicals were used as received without any purification except styrene. Styrene was purified by distillation under reduced pressure. Deionized water was used for all polymerization and treatment processes.

2.2. Synthesis of cationic polystyrene microsphere

The positively charged polystyrene (PS) cores with dimensions of 400 nm were prepared by emulsifier-free emulsion polymerization, as described by Goodwin et al. [30]. Typically, 9 g St, 2.5 g PVP, 0.5 g AIBA and 100 g deionized water were added into a 250 mL three-necked flask equipped with a mechanical stirrer at room temperature. Then the solution was deoxygenated by bubbling nitrogen gas at room temperature under continuous stirring for 1 h and stirred at 70 °C for 24 h. Then the PS was filtered and washed three times by deionized water and absolute ethanol, respectively.

2.3. Fabrication of PS/A-TiO_2 composite

Dry PS and TBOT were added into 8 mL absolute ethanol and stirred for 2 min to obtain a colloidal solution which was then transferred into VPH device (inset, Scheme 1) quickly. 3 mL deionized water was located at the bottom of VPH device as liquid phase to produce vapor at elevated temperature. The sealed VPH device was similar to normal hydrothermal synthesis reactor but with a special holder inside. Then the sealed VPH device was placed into an electric oven which can display the temperature of system. It was heated to different temperatures for 10 h and then cooled to room temperature. The detailed recipe is shown in Table 1. The PS/A-TiO_2 was collected by centrifugation and rinsed with deionized water and absolute ethanol for three times, respectively. After that, it was dried under vacuum at 60 °C for 8 h.

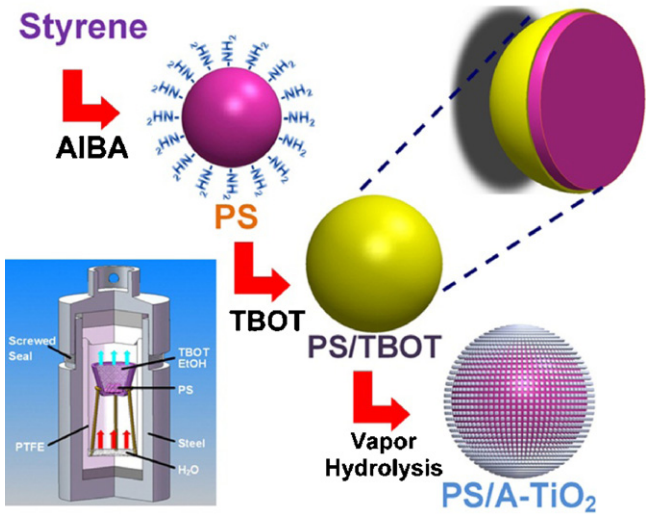

Scheme 1. Schematic representation of the fabrication procedure of PS/A-TiO_2 hybrid microspheres via vapor phase hydrolysis and the vapor phase hydrolysis device (inset).

2.4. Preparation of PS/SiO_2/A-TiO_2 photocatalyst

0.07 g dry PS and 90 μL TEOS were first added into 8 mL absolute ethanol and stirred for 2 min to obtain a colloidal solution which was then transferred into VPH device quickly. 3 mL deionized water was located at the bottom of VPH device as liquid phase to produce vapor at elevated temperature. The VPH device was heated to 150 °C for 10 h and then cooled to room temperature. The PS/SiO_2 was collected by centrifugation and rinsed with deionized water and absolute ethanol for three times, respectively. After that, 0.07 g dry PS/SiO_2 and 160 μL TBOT were also added into 8 mL absolute ethanol and the above process was repeated again. It was also heated to 150 °C for 10 h.

2.5. Synthesis of bare A-TiO_2

For comparison, bare A-TiO_2 particles were also prepared using the same method. 160 μL TBOT was added into 8 mL absolute ethanol and the above process was repeated again. The sealed VPH device was heated to 150 °C for 10 h. Bare A-TiO_2 was collected by centrifugation and rinsed with deionized water and absolute ethanol for three times, respectively. After that, it was dried under vacuum at 60 °C for 8 h. The specific surface area of bare A-TiO_2 is 94 $m^2\ g^{-1}$.

2.6. Characterization

X-ray diffraction (XRD) patterns were recorded on a Rigaku equipment (D/max 2550 PC, Rigaku Co., Japan), using Cu Kα radiation at 40 kV and 200 mA. The morphology and size of the powders were observed using transmission electron microscope (TEM) (JEM-2100F, JEOL, Japan) and high-resolution transmission electron microscope (HRTEM) with an accelerating voltage of 200 kV. Scanning electron microscopy (SEM) images were collected on S-4800 (Hitachi, Japan). The nitrogen adsorption–desorption isotherm was obtained at 77 K by nitrogen adsorption apparatus (Autosorb-1MP, Quantachrome Instruments, USA) utilizing Barrett–Emmett–Teller (BET) calculation of specific surface area and Barrett–Joyner–Halenda (BJH) calculation of pore volume and pore size (diameter) distributions from the desorption branch of the isotherm. Fourier transform infrared (FTIR) spectra were recorded by Nexus-670 (Nicolet, USA). The obtained samples were heated

in air flow from room temperature to 700 °C on a thermo gravimetric analyzer (209F1 Iris, Netzsch, Germany) at 10 °C min^{-1}. The zeta potential of particles in aqueous suspension was measured by Zetasizer Nano ZS90 (Malvern Instruments, UK).

2.7. Photocatalytic activity measurements

The photocatalytic performances of various photocatalysts were first evaluated by photocatalytic degradation of MB in Pyrex photoreactor. A set of experiments were performed as follows: desired amount of catalysts in 500 mL MB aqueous solution (15 mg L^{-1}) were magnetically stirred in the dark for 30 min to reach the adsorption equilibrium of MB with the catalyst. O_2 was bubbled into aqueous suspension at 100 mL min^{-1}. Then the suspension was irradiated using a 300 W medium-pressure Hg lamp at the wavelength of 365 nm. At different irradiation time intervals, 10 mL samples of the irradiated water were withdrawn for analysis using PerkinElmer Lambda 35 by measuring the absorbance at the wavelength of 655 nm. The degradation ratio of MB solution was calculated using Eq. (1):

$$D = \frac{C_0 - C}{C_0} \quad (1)$$

where C_0 and C are the concentration of the primal and remaining MB.

The photocatalytic oxidation of phenol was also carried out in Pyrex photoreactor, containing desired amount of samples and 500 mL phenol aqueous solution (100 mg L^{-1}). The phenol suspension containing the catalyst was stirred in the dark for 30 min to obtain the saturated absorption of phenol. O_2 was bubbled into aqueous suspension at 100 mL min^{-1}. Then the suspension was illuminated by the above Hg lamp. After different irradiation time intervals, 3 mL samples of the irradiated water were obtained by centrifugation to remove catalyst and diluted 10 times. The changes of phenol concentration were monitored by measuring the absorbance at the wavelength of 270 nm.

In order to study the long-term photocatalytic life of catalysts and the stability of the PS core, recycle experiments were carried out five times. 0.6 g Sample C or PS/SiO_2/A-TiO_2 was dispersed into 500 mL phenol solution (100 mg L^{-1}), respectively. O_2 was bubbled into aqueous suspension at 100 mL min^{-1}. The phenol suspension containing the catalyst was stirred in the dark for 30 min and then illuminated by Hg lamp for 150 min. The concentration of phenol solution was monitored using PerkinElmer Lambda 35 by measuring the absorbance at the wavelength of 270 nm after irradiation for 150 min. After being used in one cycle for 150 min, the photocatalysts were recovered by centrifugation and dried for the subsequent cycle.

3. Results and discussion

Scheme 1 illustrates the formation mechanism and the main steps involved in the preparation of PS/A-TiO_2 hybrid microspheres. The main fabrication steps are described earlier. In the first step, AIBA is used to fabricate amine-modified PS by emulsifier-free emulsion polymerization, according to Goodwin et al. [30]. AIBA ($ClH_{10}N_2C_4$–N=N–$C_4N_2H_{10}Cl$) is an azo initiator, its thermal decomposition releases nitrogen and leads to formation of the free radicals ($^{\bullet}C_4N_2H_{10}Cl$). Following reaction schemes are devised for the interaction of monomers to form the polymer chain terminal groups, Cl is dissolved in the solution and PS is terminated with –NH_2 groups. Amine modification renders the PS surface hydrophilic. In the second step, absolute ethanol with low boiling point evaporates at elevated temperature. TBOT gradually condenses to a thin layer adsorbing onto the PS surface. With continuously elevating the temperature, the water at the bottom of VPH device vaporizes and its gas gently contacts with TBOT. Then TBOT may be hydrolyzed (Eq. (2)) and polycondensed (Eqs. (3) and (4)) to form Ti–O–Ti gel as follows [31]:

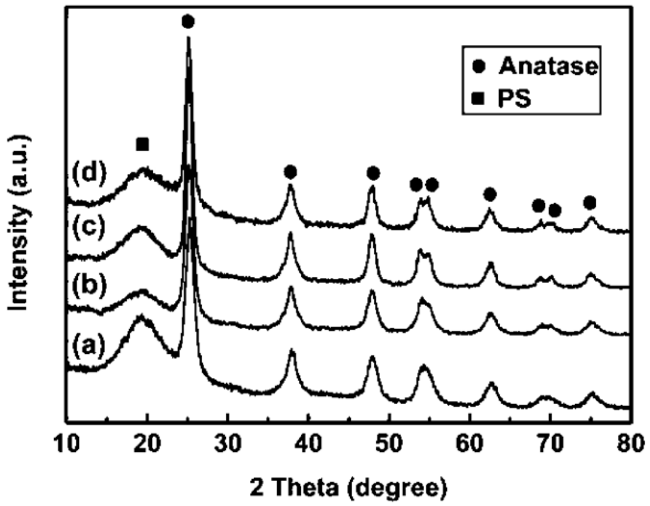

Fig. 1. XRD patterns of the different hybrid microspheres. (a) Sample A, (b) Sample B, (c) Sample C and (d) PS/SiO_2/A-TiO_2.

$$Ti(OC_4H_9)_4 + H_2O \rightarrow Ti(OH)_4 + C_4H_9OH \quad (2)$$

$$Ti(OH)_4 + Ti(OC_4H_9)_4 \rightarrow Ti\text{–}O\text{–}Ti + C_4H_9OH \quad (3)$$

$$Ti(OH)_4 + Ti(OH)_4 \rightarrow Ti\text{–}O\text{–}Ti + H_2O \quad (4)$$

At the desired temperature which is similar to that of hydrothermal treatment, TiO_2 crystallite form on the PS surface, such crystallites induce further TiO_2 deposition over time, which is similar to the seed-mediated growth [32]. It is far more difficult to synthesis ultrafine rutile using titanium alkoxide as titanium source in the absence of the concentrated strong acid such as HCl and HNO_3 or without subsequent calcination process [33,34]. Thus, the crystalline phase of TiO_2 prepared by the current process is restricted to anatase.

Table 2
The specific surface area, pore volume and crystallite size of the selected samples.

Sample	S_{BET} (m^2 g^{-1})[a]	S_{BET} (m^2 g^{-1})[b]	V_p (cm^3 g^{-1})[c]	d_{XRD} (nm)[d]
PS	16			
A	64	159	0.16	7.5
B	57	138	0.17	9.4
C	49	115	0.21	13.6
PS/SiO_2/A-TiO_2	119	–	0.18	13.6

[a] S_{BET} is the specific surface area of PS, PS/A-TiO_2 and PS/SiO_2/A-TiO_2 powders.
[b] S_{BET} is the specific surface area of A-TiO_2 in the shell through conversion.
[c] V_p is the pore volume of PS/A-TiO_2 and PS/SiO_2/A-TiO_2 powders.
[d] d_{XRD} is the crystallite size of A-TiO_2 (in the shell) estimated by Scherrer formula.

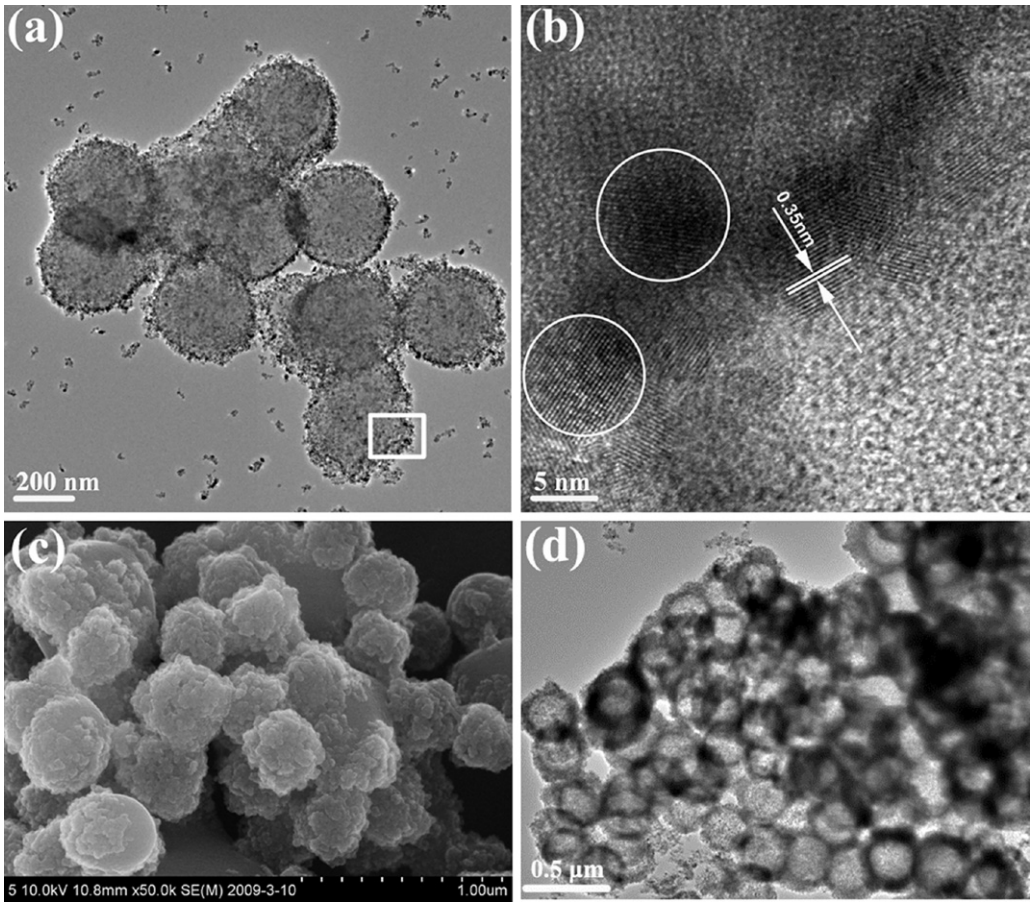

Fig. 2. TEM image (a) of Sample C; HRTEM image (b) of the selected area in (a); SEM image (c) of Sample C and TEM image (d) of the hollow titania spheres obtained by calcining Sample C at 500 °C for 2 h.

Fig. 1 shows the XRD spectra of the selected samples. Amorphous and crystalline phase are both obvious in the selected samples. All crystalline peaks could be assigned to well-crystalline anatase TiO_2 (JCPDS No. 21-1272). It is clear seen from XRD patterns that all samples exhibit peak broadening. Calculating through the diffraction peak at $2\theta = 25.3^\circ$ using Scherer formula, the crystallite sizes of A-TiO_2 in Sample A, Sample B, Sample C and PS/SiO_2/A-TiO_2 are to be ca. 7.5 nm, 9.4 nm, 13.6 nm and 13.6 nm, respectively. Table 2 summarizes the different parameters of the samples prepared under various temperatures, which indicating that the higher temperature results in larger crystallite. Four broad peaks ranging in 15–30° are almost same and can be assigned to amorphous polystyrene. It is implied that PS and crystalline A-TiO_2 coexist in all samples, and VPH method avoids the loss of PS through calcination. Because of the amorphous nature of SiO_2, the SiO_2 peak may superpose with the PS peak. The peak position and intensity of curve c and curve d are almost same.

The morphologies of as-synthesized samples are revealed by TEM and SEM. Although the reaction temperature is higher than the glass transition temperature (T_g) of PS (~100 °C) and the pressure holds in excess of 1 atm. for 10 h, the temperature is far below the melting point of PS (240 °C) and PS is still in solid state. As a result, there is limited damage to PS. Fig. 2(a) shows the PS microsphere is uniform with diameter around 400 nm. After the surface coated with a thick layer (20–50 nm) of polycrystalline A-TiO_2, microspheres retain their spherical structure but have far rougher surfaces. Fig. 2(a) also shows the average particle size of Sample C is around 450 nm. Crystallinity and crystallite size of A-TiO_2 are further confirmed by HRTEM image, as shown in Fig. 2(b). The circles marked in Fig. 2(b) indicate that the crystallite size of A-TiO_2 is around 13 nm, which agrees the calculation of XRD (Table 2). The clear lattice fringe of 0.35 nm showed in Fig. 2(b) is assigned to the (1 0 1) plane of A-TiO_2. Fig. 2(c) shows A-TiO_2 is uniformly coated on the PS surface of PS. The PS/A-TiO_2 microsphere in the lower left quarter of Fig. 2(c) gives the detailed information of the smooth PS surface and the rough polycrystalline A-TiO_2 shell. Sample C is then subjected to calcination at 500 °C for 2 h, and the remaining hollow spheres are shown in Fig. 2(d). A few hollow TiO_2 shells break down during calcination, but most of them retain intact.

In order to demonstrate the existence of SiO_2 insulating coating, the ζ-potential profiles of cationic PS, PS/SiO_2 and PS/SiO_2/A-TiO_2 microspheres in the pH range of 1–14 are compared in Fig. 3. The isoelectric points of SiO_2 and TiO_2 are in the ranges of 2–2.5 [35] and 5–7 [36], respectively. And the curves give an isoelectric point at 3.5 for PS/SiO_2, 4.4 for PS/SiO_2/A-TiO_2 and 10.9 for PS. It reveals a tremendous shift of isoelectric point from 10.9 to 3.5 and then to 4.4, suggesting the uniformity of silica and titania layers. The weight ratio of A-TiO_2 in the composite is measured by thermogravimetric analysis. As shown in Fig. 4, PS spheres exhibit two main weight losses associated with elevated temperature. The weight loss below 400 °C is attributed to evaporation of physically adsorbed water and solvent residual, while the weight loss above 400 °C is attributed to PS decomposition. There is no further weight loss at temperature higher than 430 °C. The PS decomposition temperature region (400–450 °C) in Sample D, Sample C and Sample E is similar to that of PS. The relative weight losses suggest the weight ratios of A-TiO_2 are 27.1 wt%, 33.5 wt% and 45.7 wt% in Sample D, Sample C and Sample E, respectively. With increasing the TBOT content, the

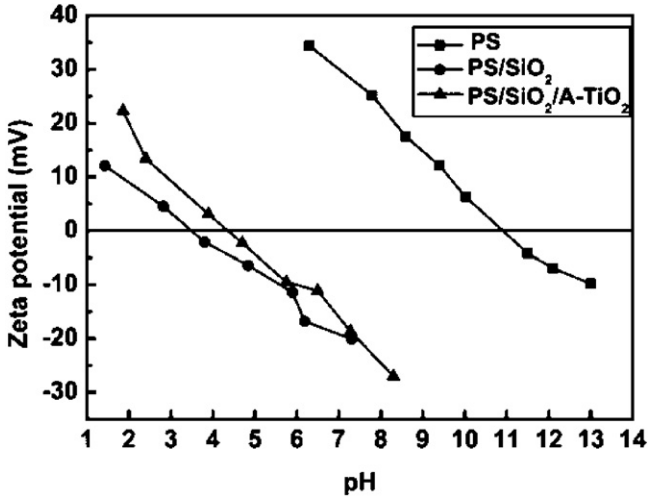

Fig. 3. Zeta potential profiles as a function of pH for the cationic PS, PS/SiO_2 and $PS/SiO_2/A\text{-}TiO_2$ microspheres.

weight ratio of $A\text{-}TiO_2$ increases and $A\text{-}TiO_2$ distributes on the PS surface. Thus, the thickness of $A\text{-}TiO_2$ shell could be controlled by varying the TBOT content [37]. Assuming the densities of $A\text{-}TiO_2$ (3.84 g cm^{-3}) and PS (1.04 g cm^{-3}), the density of Sample C containing 33.5 wt% $A\text{-}TiO_2$ is calculated to be 1.41 g cm^{-3}. This value is much lower than that of $A\text{-}TiO_2$. Considering the porous nature of $A\text{-}TiO_2$ shell (Fig. 4(b)), the density of the composite is even lower than 1.41 g cm^{-3}. The weight ratios of SiO_2 in PS/SiO_2 and $SiO_2/A\text{-}TiO_2$ in $PS/SiO_2/A\text{-}TiO_2$ are also obtained to be 24.5 wt% and 56.3 wt% by TG analysis. This means the weight ratios of PS in PS/SiO_2 and $PS/SiO_2/A\text{-}TiO_2$ are 75.5 wt% and 43.7 wt%, respectively. Considering the weight ratio of SiO_2 in PS/SiO_2 (24.5 wt%), one could calculate the weight ratios of SiO_2 and $A\text{-}TiO_2$ in $PS/SiO_2/A\text{-}TiO_2$ composite are 14.2 wt% and 42.1 wt%, respectively.

FTIR spectra shown in Fig. 5(a) demonstrate that only physical adsorption between PS and $A\text{-}TiO_2$ which exist in the composite. PS microspheres show bands at around 3000 cm^{-1} and 1470 cm^{-1}, associated with the phenyl C–H stretching and C–C stretching vibrations, respectively. Peaks at around 760 cm^{-1} and 700 cm^{-1} are associated with phenyl C–H and C–C bending vibrations out of the phenyl plane, respectively. Peaks at 3400 cm^{-1} and 650 cm^{-1} are characteristic of hydroxyl groups and adsorbed water. Large differences between the three curves indicate that PS and $A\text{-}TiO_2$ co-exist in the composite. Table 2 gives some specific surface area of the selected samples. The specific surface area of Sample C is 49 m^2 g^{-1}. Considering the contribution of the specific surface area of PS (16 m^2 g^{-1}) and weight ratio of $A\text{-}TiO_2$ in the composite (33.5 wt%), the specific surface area of titania shell is calculated to 115 m^2 g^{-1}. Table 2 also indicates the fact that the specific surface area of the samples decreases with increasing the preparative temperature because the higher temperature results in larger crystallite. Inset of Fig. 5(b) are the pore-size distributions of Sample A, Sample B and Sample C. The pore volumes (V_p) range from 0.16 cm^3 g^{-1} to 0.21 cm^3 g^{-1} and pore diameters range from 6.7 nm to 9.6 nm which mainly resulted from TiO_2 nanocrystallites packing in the shell. The adsorption isotherm in Fig. 5(b) exhibits a type IV curve with a H3 hysteresis loop, which is characteristic of mesopores in the spherical shell. Such a mesoporous structure of the shell could promote the molecule adsorption in pollutants.

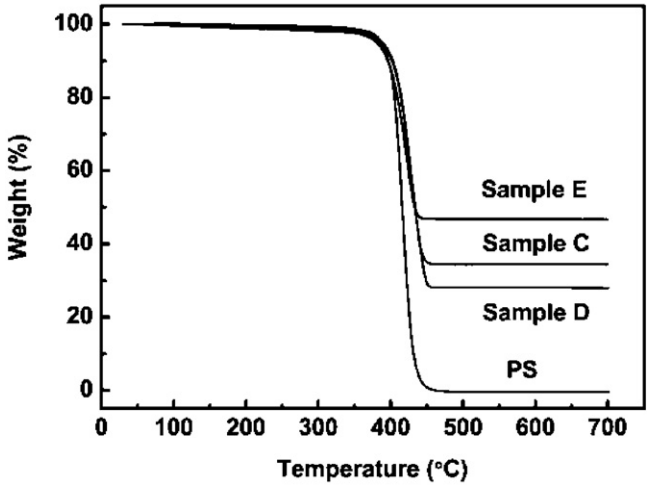

Fig. 4. TG curves of PS and $PS/A\text{-}TiO_2$ microspheres.

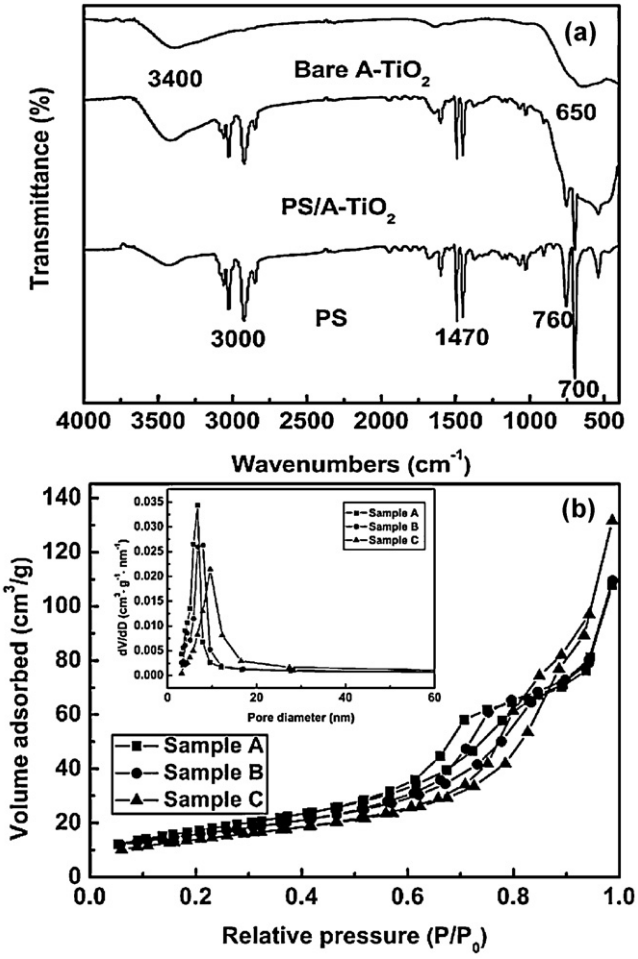

Fig. 5. FTIR spectra (a) of PS, bare $A\text{-}TiO_2$ and Sample C; N_2 adsorption–desorption isotherm (b) of $PS/A\text{-}TiO_2$ hybrid microspheres at 77 K with corresponding pore size distributions (inset) calculated by Barrett–Joyner–Halenda (BJH) method from desorption branch.

UV–vis diffuse reflectance spectra of $PS/A\text{-}TiO_2$ and bare $A\text{-}TiO_2$ powders are shown in Fig. 6(a). There is only 33.5 wt% $A\text{-}TiO_2$ contained in Sample C, and all titania crystallites distribute on the PS surface, but the absorbance at the wavelength of 300 nm is almost the same as bare $A\text{-}TiO_2$, whose centric area of particle is difficult to be irradiated by light. This demonstrates the $PS/A\text{-}TiO_2$ composites exhibit better light harvesting property than bare $A\text{-}TiO_2$. The different titania distribution also gives rise to the suspension with different extinction (absorption and scattering) characteristics. Fig. 6(b) shows the extinction (absorption and scattering)

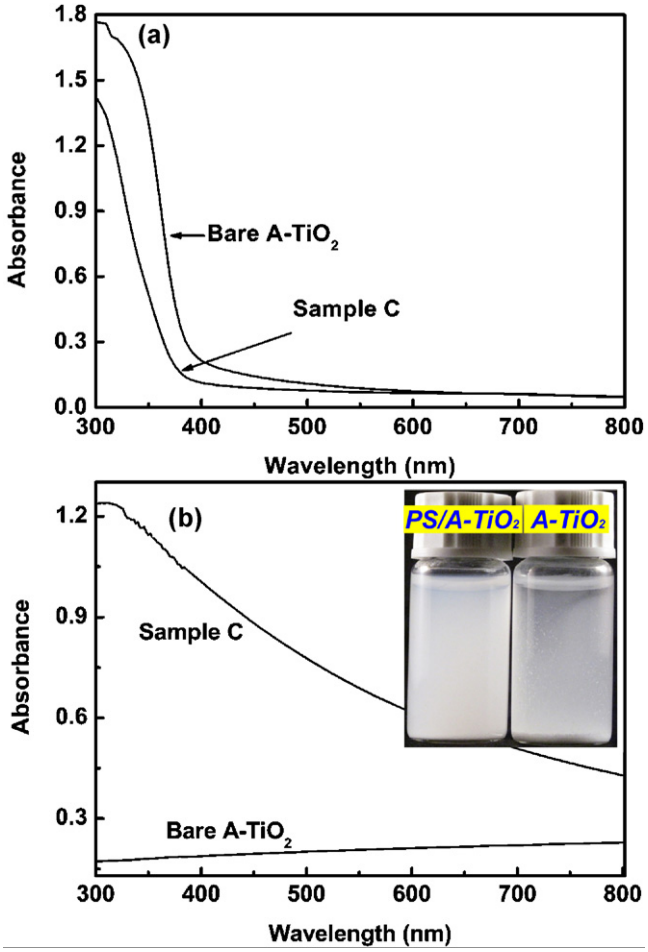

Fig. 6. UV–vis diffuse reflectance spectra (a) of bare A-TiO_2 and Sample C; the extinction (absorption and scattering) spectra (b) of 1 mM diluted suspensions of the selected samples and the colloidal stability (inset) of bare A-TiO_2 and Sample C suspensions after standing for 2 h.

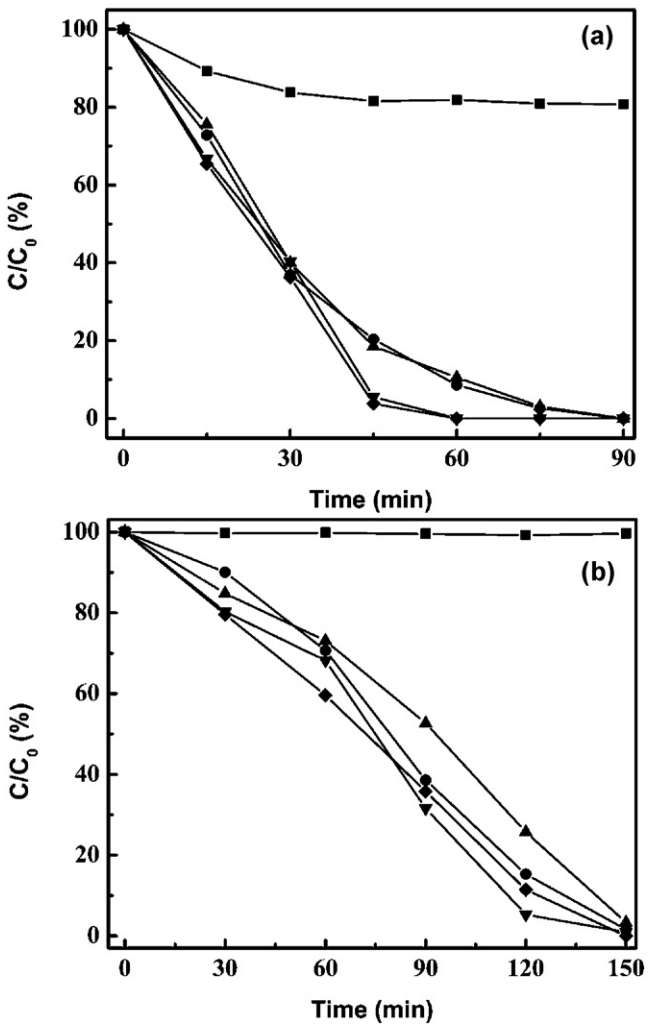

Fig. 7. The degradation rates of MB (a) and phenol (b) solution photocatalyzed by different samples. Catalyst loading: (■) no catalyst, (●) 0.2 g bare A-TiO_2, (▲) 0.2 g Sample C (denoted as Sample C-I), (▼) 0.6 g Sample C (denoted as Sample C-II) and (♦) 0.47 g PS/SiO_2/A-TiO_2.

spectra of bare A-TiO_2 and Sample C suspensions. The suspension of Sample C absorbs and scatters more light in UV–vis region, which may due to the transparency of PS and fine A-TiO_2 crystallites located on the PS surface. Bare A-TiO_2 suspension absorbs and scatters less light due to the aggregation; it is difficult for occluded TiO_2 spheres to utilize the light efficiently which agrees with the result of UV–vis diffuse reflectance spectra. The colloidal stability of Sample C and bare A-TiO_2 are shown in the inset of Fig. 6(b). 5 mg bare A-TiO_2 and Sample C are dispersed into 10 mL deionized water and placed still after sonication for 5 min. The result indicates the PS/A-TiO_2 particles are more stable than bare A-TiO_2 in deionized water after standing for 2 h. This phenomenon also verifies the density of Sample C is lower than A-TiO_2, in accordance with the TG analysis.

The photodegradation of MB is selected as a model reaction to investigate the photocatalytic activity of the selected samples. The photocatalytic performances of various catalysts in MB solution is monitored at 655 nm and shown in Fig. 7(a). In the absence of catalyst, the decoloring ratio of MB is less than 20% due to the irradiation of UV light [38]. Due to the easy degradation of MB, the final degradation ratios of PS/SiO_2/A-TiO_2, Sample C-II, Sample C-I and A-TiO_2 are all of 100% after UV irradiation for 90 min. Although the amount of TiO_2 is same, PS/SiO_2/A-TiO_2 and Sample C-II give a faster photocatalytic rates than that of bare A-TiO_2 due to the distribution of A-TiO_2 and utilizing efficiency of light. There is no obvious difference in the photocatalytic performances of PS/SiO_2/A-TiO_2 and Sample C-II. Owning to the different amount of TiO_2, the photocatalytic rate of PS/SiO_2/A-TiO_2 or Sample C-II exceeds that of Sample C-I. The degradation rates of phenol solution photocatalyzed by different samples are also evaluated under UV irradiation. Fig. 7(b) shows the photocatalytic performances of various catalysts in phenol. In the absence of catalyst, the degradation ratio of phenol almost has no changes during the UV irradiation process. The final degradation ratio of Sample C-II (100%) is higher than that of bare A-TiO_2 (98.4%) and Sample C-I (96.7%). Sample C-II also shows a higher photocatalytic rate than bare A-TiO_2 or Sample C-I, which can be explained according to that mentioned in the degradation of MB. The amount of TiO_2 is same in bare A-TiO_2, Sample C-II and PS/SiO_2/A-TiO_2, but A-TiO_2 in Sample C-II or PS/SiO_2/A-TiO_2 is all located on the PS surface. This could make it interact with phenol completely and be irradiated efficiently. The photocatalytic rate of PS/SiO_2/A-TiO_2 is slightly lower than that of Sample C-II, may arise from the SiO_2 insulating layer reduces the utilizing efficiency of the light.

In order to study the long-term photocatalytic life of catalysts and the stability of the PS core, recycle experiments were carried out five times. Fig. 8 shows the recycle degradation ratios of Sample C and PS/SiO_2/A-TiO_2 in phenol solution. Phenol is completely removed from the solution after the first cycle by treating with

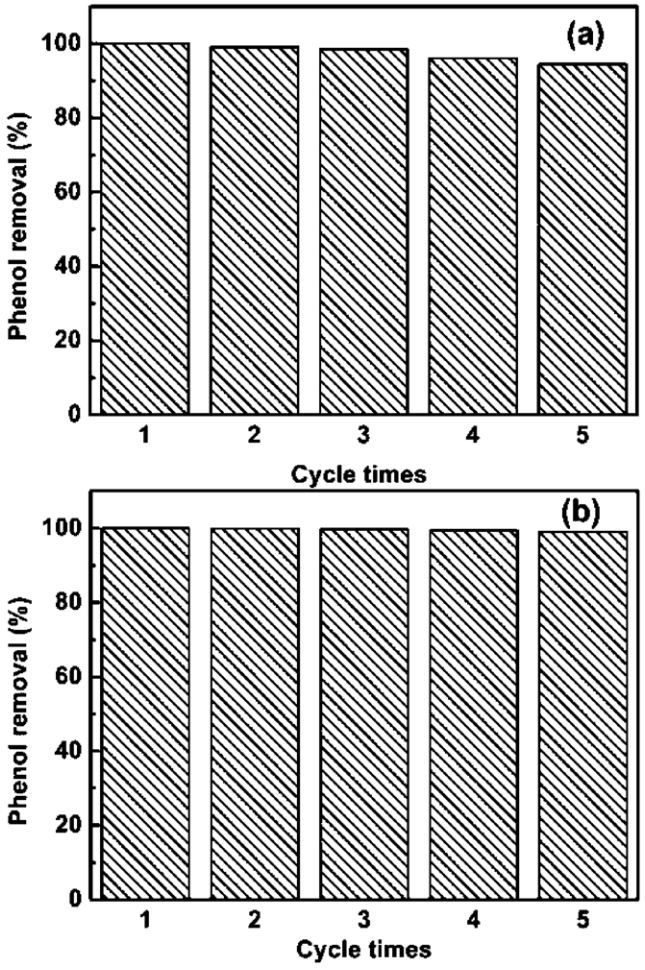

Fig. 8. The recycle degradation ratios of the selected samples in phenol solution. Catalyst loading: (a) 0.6 g Sample C and (b) 0.6 g PS/SiO_2/A-TiO_2.

Sample C. However, the photocatalytic activity of Sample C slightly decreases with increasing the cycle numbers. The degradation ratio decrease to 94.5% and the color of PS/A-TiO_2 photocatalyst transfers from white to light yellow after five cycles. In comparison, the final degradation ratio of phenol photocatalyzed by PS/SiO_2/A-TiO_2 has no changes during the 5 cycles due to the insulating coating of SiO_2 as blocking layer between the PS core and photocatalytic TiO_2 shell. This illustrates that PS has consumed some active radicals, which are generally used in the photocatalytic oxidation of MB, phenol or their intermediate derivatives.

4. Conclusions

In summary, the core/shell structured PS/A-TiO_2 photocatalyst has been prepared by a vapor phase hydrolysis process, and the thickness of A-TiO_2 shell can be tuned from monolayer to several hundred nanometers by varying the TBOT content. To the best of our knowledge, this is the first report that crystalline A-TiO_2 has been coated onto the surface of polymer microsphere in the absence of surfactant. Although PS/A-TiO_2 has a higher activity than bare A-TiO_2 due to the crystalline nature of TiO_2 shell, better floating ability and improved light harvesting property. The PS core has competitively consumed some active radicals, which are generally essential to the photocatalytic oxidation of MB, phenol or their intermediate derivatives. After introducing the insulating coating of SiO_2 between the PS core and photocatalytic TiO_2 shell, it can retain its high photocatalytic efficiency and the long-term stability of PS/A-TiO_2 composite is also enhanced.

Acknowledgements

This research is supported by the National Natural Science Foundation of China (No. 50772127, No. 50772022 and No. 50925312), the Opening Project of State Key Laboratory of High Performance Ceramics and Superfine Microstructure (No. SKL201002SIC), the Cultivation Fund of the Key Scientific and Technical Innovation Project (No. 708039), and the Program of Introducing Talents of Discipline to Universities (No. 111-2-04).

References

[1] H. Zou, S.S. Wu, J. Shen, Chemical Reviews 108 (2008) 3893.
[2] M. Chen, S.X. Zhou, B. You, L.M. Wu, Macromolecules 38 (2005) 6411.
[3] M. Agrawal, S. Gupta, M. Stamm, Journal of Materials Chemistry 21 (2011) 615.
[4] J.L. Yin, X.F. Qian, J. Yin, Y.B. Zhang, J.C. Zhang, M.W. Shi, G.T. Zhou, Journal of Solid State Chemistry 177 (2004) 3603.
[5] F.F. Fang, J.H. Kim, H.J. Choi, Polymer 50 (2009) 2290.
[6] X.J. Fang, H. Yang, G. Wu, W.G. Li, H.Z. Chen, M. Wang, Current Applied Physics 9 (2009) 755.
[7] J.K. Park, J.K. Kim, H.K. Kim, Journal of Materials Processing Technology 186 (2007) 367.
[8] Y.Y. Song, F. Schmidt-Stein, S. Bauer, P. Schmuki, Journal of the American Chemical Society 131 (2009) 4230.
[9] E.S. Kwak, W. Lee, N.G. Park, J. Kim, H. Lee, Advanced Functional Materials 19 (2009) 1093.
[10] S. Shanmugam, A. Gabashvili, D.S. Jacob, J.C. Yu, A. Gedanken, Chemistry of Materials 18 (2006) 2275.
[11] Q.H. Zhang, W.G. Fan, L. Gao, Applied Catalysis B 76 (2007) 168.
[12] G. Liu, X.X. Yan, Z.G. Chen, X.W. Wang, L.Z. Wang, G.Q. Lu, H.M. Cheng, Journal of Materials Chemistry 19 (2009) 6590.
[13] S.C. Yang, D.J. Yang, J. Kim, J.M. Hong, H.G. Kim, I.D. Kim, H. Lee, Advanced Materials 20 (2008) 1059.
[14] H.S. Li, Y.P. Zhang, S.Y. Wang, Q. Wu, C.H. Liu, Journal of Hazardous Materials 169 (2009) 1045.
[15] X.F. Song, L. Gao, Journal of Physical Chemistry C 111 (2007) 8180.
[16] J. Zhou, M. Chen, X.G. Qiao, L.M. Wu, Langmuir 22 (2006) 10175.
[17] Z. Ding, X.J. Hu, G.Q. Lu, P.L. Yue, P.F. Greenfield, Langmuir 16 (2000) 6216.
[18] L.Z. Wang, Y. Ebina, K. Takada, T. Sasaki, Journal of Physical Chemistry B 108 (2004) 4283.
[19] P. Wang, D. Chen, F.Q. Tang, Langmuir 22 (2006) 4832.
[20] X.F. Song, L. Gao, Langmuir 23 (2007) 11850.
[21] I.B. Jang, J.H. Sung, H.J. Choi, I. Chin, Synthetic Metals 152 (2005) 9.
[22] P.H. Mutin, A. Vioux, Chemistry of Materials 21 (2009) 582.
[23] T. Katou, D.L. Lu, J.N. Kondo, K. Domen, Journal of Materials Chemistry 12 (2002) 1480.
[24] M. Niederberger, Accounts of Chemical Research 40 (2007) 793.
[25] G. Dagan, M. Tomkiewicz, Journal of Physical Chemistry 97 (1993) 12651.
[26] Z.H. Zhang, X.H. Zhong, S.H. Liu, D.F. Li, M.Y. Han, Angewandte Chemie-International Edition 44 (2005) 3466.
[27] J. Joo, S.G. Kwon, T. Yu, M. Cho, J. Lee, J. Yoon, T. Hyeon, Journal of Physical Chemistry B 109 (2005) 15297.
[28] M. Niederberger, M.H. Bartl, G.D. Stucky, Journal of the American Chemical Society 124 (2002) 13642.
[29] C.T. Dinh, T.D. Nguyen, F. Kleitz, T.O. Do, ACS Nano 3 (2009) 3737.
[30] J.W. Goodwin, R.H. Ottewill, R. Pelton, Colloid and Polymer Science 257 (1979) 61.
[31] C.C. Wang, J.Y. Ying, Chemistry of Materials 11 (1999) 3113.
[32] B. Nikoobakht, M.A. El-Sayed, Chemistry of Materials 15 (2003) 1957.
[33] K. Terabe, K. Kato, H. Miyazaki, S. Yamaguchi, A. Imai, Y. Tguchi, Journal of Material Science 29 (1994) 1617.
[34] X.Z. Ding, Z.Z. Qi, Y.Z. He, Journal of Materials Science Letters 14 (1995) 21.
[35] S. Hermes, D. Zacher, A. Baunemann, C. Woll, R.A. Fischer, Chemistry of Materials 19 (2007) 2168.
[36] D. Gumy, C. Morais, P. Bowen, C. Pulgarin, S. Giraldo, R. Hajdu, J. Kiwi, Applied Catalysis B 63 (2006) 76.
[37] M.S. Cho, Y.H. Cho, H.J. Choi, M.S. Jhon, Langmuir 19 (2003) 5875.
[38] Z.L. Wang, L.Q. Mao, J. Lin, Journal of Photochemistry and Photobiology A 177 (2006) 261.